Acoustic impedance and interface phonon scattering in Bi_{2}Te_{3} and other semiconducting materials

Xin Chen, David Parker, and David J. Singh

Phys. Rev. B **87**, 045317 — Published 30 January 2013

DOI: 10.1103/PhysRevB.87.045317

Acoustic impedance and interface phonon scattering in Bi_2Te_3 and other semiconducting materials

Xin Chen, David Parker and David J. Singh
Oak Ridge National Laboratory, 1 Bethel Valley Rd., Oak Ridge, TN 37831
(Dated: January 18, 2013)

We present first principles calculations of the phonon dispersions of Bi_2Te_3 , along with calculations of the sound speed anisotropy for a number of materials, and discuss these in relation to the acoustic phonon interface scattering in ceramics. The Bi_2Te_3 phonon dispersions show agreement with what is known from neutron scattering for the optic modes, while we find a difference between the generalized gradient approximation and local density results for the acoustic branches. This is a consequence of an artificial compression of the van der Waals bonded gaps in the Bi_2Te_3 structure when using the generalized gradient approximation. As a result local density approximation calculations provide a better description of the phonon dispersions in Bi_2Te_3. A key characteristic of the acoustic dispersions in several materials studied is the existence of a strong anisotropy in the velocities. Such an anisotropy may be a significant consideration in the reduction of lattice thermal conductivity by nanograin boundary scattering. This is a well-known technique commonly employed to improve thermoelectric performance. We develop a model to quantify the effect of this anisotropy for this interface scattering in ceramics and apply this to Bi_2Te_3 and compare with PbTe and several other semiconductors.

I. INTRODUCTION

Thermoelectric performance is commonly quantified in terms of a dimensionless parameter ZT, defined as follows:

$$ZT = \frac{S^2 \sigma T}{\kappa} \tag{1}$$

Here S is the Seebeck coefficient, σ the electrical conductivity, and κ the thermal conductivity. It is usually a good approximation to treat κ as being comprised of a lattice portion and an electronic portion. The electronic portion is directly related to the electrical conductivity by the Wiedemann-Franz relation (usually a good approximation for the heavily doped semiconductors that are useful thermoelectrics), leading to the point that, from a standpoint of materials optimization, the lattice thermal conductivity represents wasted heat transfer and should be as small as possible. One realization of this is the "phonon glass electronic crystal" (PGEC) concept of Slack[1], in which phonons are strongly scattered, leading to low lattice thermal conductivity, while the charge carriers are not strongly scattered. The filled skutterudites[2–4] represent an apparent realization of the PGEC concept. Another approach towards the PGEC concept is the use of nanostructuring from compaction and sintering of a nanosize powder into a ceramic. The mean free path for phonons in bulk crystalline thermoelectrics is often one to two orders of magnitude larger than that for electrons, so the use of grain sizes in between these two mean free paths will tend to strongly scatter phonons, but not electrons. This approach has been successfully applied to Bi_2Te_3[5,6], raising the ZT values near room temperature from the previously found value of 1.0 to an impressive 1.5. A similar scenario could also apply to hole-doped Bi_2Se_3[7]. Note that there are various types of grain boundary scattering that can reduce the thermal conductivity, such as insulating interstitial material, but typically these destroy the electrical conductivity, preventing good thermoelectric performance. In this respect, the sintering of polycrystalline samples (as opposed to simply compressed powder) is important as it assures good electrical contact between the nanograins, while maintaining interface scattering. Understanding interface phonon scattering at such electrically conducting interfaces is therefore of importance.

One factor as yet unaddressed, however, is the role of phononic anisotropy in producing phononic scattering. Consider by analogy, for example, the case of light propagation in dense ceramics. In that case it is known that fine-grained ceramics of optically isotropic materials can be made transparent[8], while this is not the case for anisotropic materials with random grain orientation. In the former case, despite the small grain sizes, light is able to pass through the material because there is not significant scattering at the grain boundaries. The reason for this is that the light speed does not change at the grain boundary, so there is no impedance (or velocity) mismatch. While the acoustic case differs from the optical case due to the presence of the longitudinal mode, the velocity mismatch still applies.

We note also that, unlike in optics where there is no optical anisotropy in cubic materials, a cubic material can have a rather anisotropic elastic response tensor (the tensor of elasticity C_{ijkl}) and hence sound speed - a good example of such a material is PbTe, as described in more detail in the last section. This material shows comparable anisotropy to Bi_2Te_3 despite being cubic. The reason for this is that the response tensor for optics - the dielectric constant tensor - is a *second* rank tensor whose off-diagonal elements must necessarily vanish due to the cubic symmetry. However, no such restriction applies to the *fourth* rank-tensor of elasticity, and indeed the sound velocity in a cubic material can vary significantly by direction, as will be evident for PbTe.

Note that for heat transport in crystalline solids it is the longer wavelength acoustic modes that dominate heat transport due to the presence of a significant group velocity - the sound speed. The main point of this paper is that it is this sound velocity mismatch that is ultimately responsible for the efficacy of grain boundary scattering, and that this mismatch can be quantitatively assessed by considering the sound velocity anisotropy. We are here working in the limit in which the phonon mean free path is larger than the nanograin size, so that transport within a grain is in the ballistic limit, as was considered in a different context in Ref. 9. In this limit the lattice thermal conductivity will be predominated by the size of the nanograins and not the diffusive scattering as was considered in Ref. 10.

We provide a definition, and examples of, simple dimensionless parameters R and S, easily computable if the elastic constants are known, that should provide valuable information about the ability of nanostructuring (of a type that yields grains in intimate contact) to reduce lattice thermal conductivity.

We will make direct application of our findings to Bi_2Te_3, which as already mentioned has already shown substantial performance benefits from nanostructuring, and in addition PbTe and several other semiconductors. One conclusion to be drawn from our work is that, unlike in electronic transport, where anisotropy can be destructive to thermoelectric performance, in phononic transport anisotropy is generally beneficial by enhancing the effects of nanostructuring in reducing the lattice thermal conductivity.

II. PHONON AND ELASTIC CONSTANT CALCULATIONS FOR BI_2TE_3

With an eye towards the effects of nanostructuring in reducing $\kappa_{lattice}$ and enhancing ultimate performance we have computed the phonon dispersions and density-of-states for Bi_2Te_3, the best known and most studied thermoelectric. Our calculations are

TABLE I. Calculated elastic constants (in GPa) for Bi_2Te_3

Approximation	c_{11}	c_{12}	c_{13}	c_{33}
LDA	83.8	3.8	32.1	54.5
GGA	97.4	21.4	—	90.4

based upon density functional theory in the framework of Blöchl's projector augmented-wave (PAW) method[11] within the local density approximation (LDA) as implemented in VASP[12]. We also did generalized gradient approximation calculations but found that they are not as accurate as the LDA results (see below). A 3x3x3 *k*-point grid in a 3x3x3 supercell was used, along with an energy cutoff of 300 eV. Cell parameters (and internal coordinates were both relaxed until internal forces were less than 2 meV/Å. From the computed electronic structure one performs several supercell calculations incorporating "frozen-phonons", or atomic displacements dictated by the rhombohedral crystal symmetry. By evaluating the forces on the displaced atoms one may generate a basis set of force constants from which the phonon band structure and density-of-states are generated. We depict these in Figure 1. Previous Bi_2Te_3 lattice dynamics calculations were performed in Refs. 13–16. Spin orbit coupling was not included and we therefore cannot assess the claim of Ref. 15 for evidence of a spin-orbit coupling-related lattice instability. Experimentally the material is known to be stable. Our calculations generally reproduce the non spin-orbit coupling phonon dispersions of these authors.

One notes upon examination of the central region (the portions Z-Γ and Γ-L) that the three acoustic modes differ significantly in these two directions (respectively c-axis and in-plane). In particular, the highest velocity acoustic mode, the longitudinal acoustic, has significantly lower velocity in the c-axis direction $\Gamma - Z$ than the nearly planar direction $\Gamma - L$; quantitatively, the c-axis longitudinal velocity is 1811 m/sec and the planar is 2394 m/sec, a difference of about 30 percent. In addition, the transverse acoustic modes are degenerate from Γ-Z but not so in plane; here the velocities are significantly different as well, with the single c-axis value of 1774 m/sec and the two planar velocities of 1395 and 1728 m/sec. These velocities are low and generally typical of good thermoelectric materials. Note also that in the frequency range at and above 1 THZ the optic modes intersect with the acoustic modes, so that the primary region of heat transport is limited to less than 1 THZ, which in turn limits the phonon momenta that contribute to transport to locations relatively near the Γ point.

Turning to the phonon density of states, one finds three regions of interest. Highest in frequency, as expected given the lighter mass, are the primarily Te optic modes between 2.3 and 4 THZ. As noted previously, these modes are not the primary contributors to phononic transport due to the very small group velocities (see left hand panel of Fig. 1), although they do make some contribution. A similar statement applies to the primarily Bi optic modes between 1 and 2.3 THZ ,although these may be important contributors to phononic scattering due to anharmonic scattering of the lower frequency acoustic modes, which are at frequencies less than 1.5 THZ. As noted above, only a fraction of these modes - those less than 1 THZ - contribute to thermal transport as the higher frequency acoustic modes are strongly scattered by the adjacent optic modes, and also have smaller group velocities. For example, in the $\Gamma - L$ direction only those acoustic phonons less than half the L-point momentum will strongly contribute to heat transport, while in the $\Gamma - F$ direction this cut-off frequency occurs at a momentum roughly sixty percent of the F-point momentum. It is to be noted that the later discussion of sound speed anisotropy as a contributor to nanograin scattering is an approximation which effectively assumes that *all* phononic transport derives from the acoustic modes, which is clearly somewhat simplified compared to reality, as the optic modes in Figure 1 do in fact exhibit some dispersion and hence heat transport. Nevertheless it is likely that the majority of transport indeed derives from the acoustic modes.

The original lattice dynamics calculations for this work employed the standard GGA[17,18]. However, these results produced longitudinal sound speed velocities which were higher in the Γ-Z direction (the c-axis) than in the planar directions. This result persisted even when a relatively fine 4x4x4 *k*-point mesh was used. Similarly, we initially found from first principles calculations of the elastic constants of Bi_2Te_3 using WIEN2K[19] and the GGA that the elastic constant c_{11} and c_{33} are very nearly equal. All these results are contrary to the elastic constant data of Jenkins[20], which produces higher longitudinal sound speeds in-plane (see the next section), as well as the measured planar and c-axis thermal conductivity[21], where the c-axis value is less than half the planar value, indicating lower c-axis sound speeds. Our calculational discrepancy was likely due to the common GGA overestimation of lattice constants. It was for this reason that we performed these lattice dynamics calculations within the LDA, which often gives structural and elastic properties in better agreement with experiment[22,23]. These results suggest that for anisotropic layered semiconductors such as Bi_2Te_3, use of the LDA to compute elastic and lattice dynamics properties may be desirable.

For a direct comparison with experiment, included in Figure 1 are plots of the phonon dispersions deduced by Jenkins. While exact in-plane comparisons are not possible due to Jenkins' choice of $\Gamma - X$ and $\Gamma - Y$ dispersion directions, we note that as in our calculated results the $\Gamma - Z$ sound speed is lower than the planar values. In general there is a reasonable correspondence between Jenkins' results and ours, with the $\Gamma - Z$ acoustic modes reaching values of $\sim 0.8 - 1$ THZ in both cases (note that Jenkins' data is presented in rad/sec whereas ours is in Hertz). AT the Z point, Jenkins' optic mode frequencies are 7,9, 17, 21, 23 and 27 $\times 10^{12}$ rad/sec, which compare rather well with our values of 1.2,1.6, 2.7, 3.3, 3.5 and 4.5 THZ. At the Γ point, Jenkins' optic

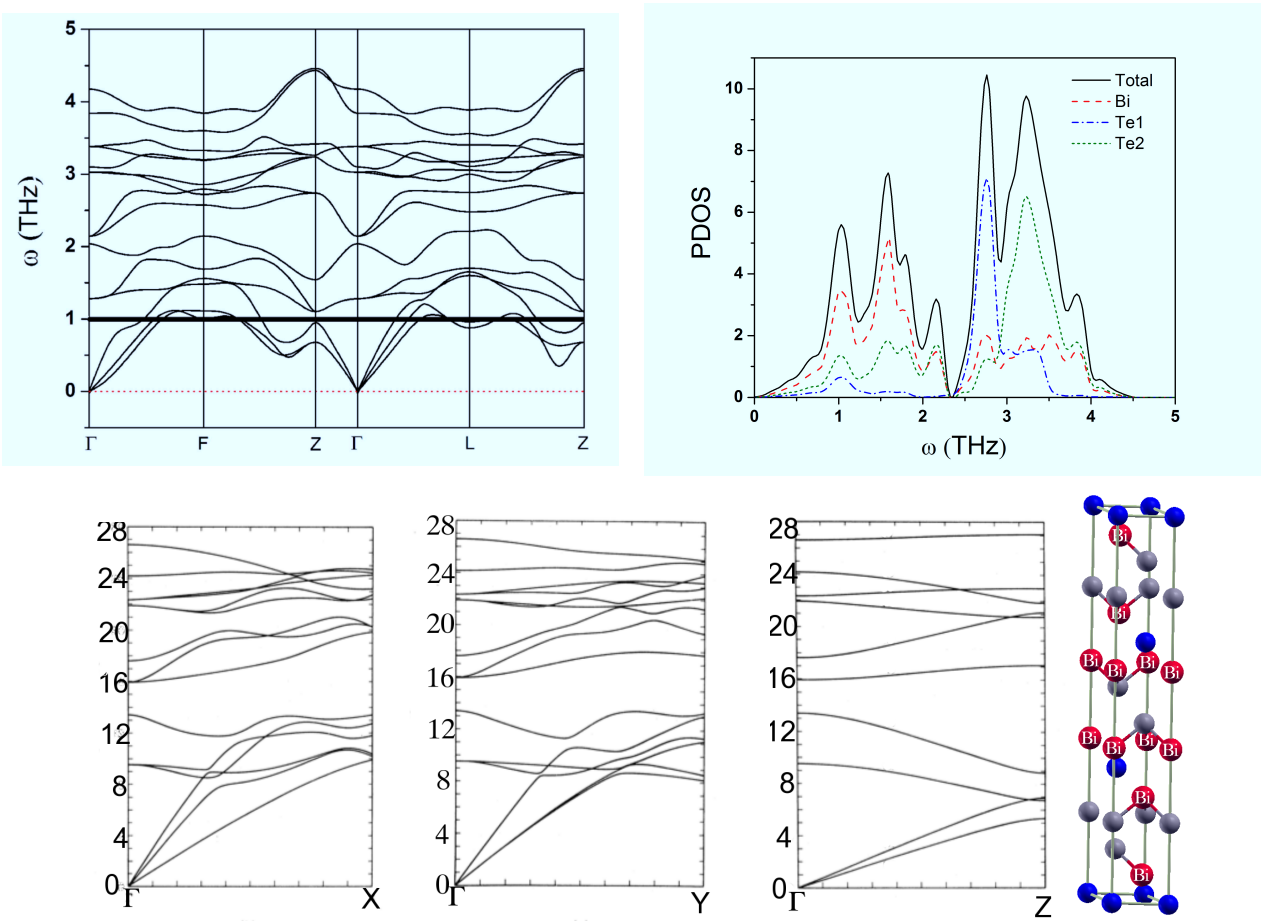

FIG. 1. The computed phonon dispersions (top left) and associated density-of-states (top right) of Bi_2Te_3. Coordinate momenta (units of reciprocal rhombohedral lattice vector) : L : (1/2,0,0); F : (1/2,0,1/2) Z: (1/2,1/2,1/2). The heavy black line in the left figure indicates the upper frequency limit of the predominant heat carrying acoustic modes. Bottom: the measured phonon dispersions, in THZ, from Ref. 20 and a picture of the physical structure of Bi_2Te_3. Phonon dispersions from left: $\Gamma - X, \Gamma - Y, \Gamma - Z$. In structure picture, Te1 is in blue (located at top and bottom) and Te2 in grey (second layer from top and bottom).

mode frequencies are approximately 9.5, 13.5, 16,17.7, 22,22.5,24 and 26.5 $\times 10^{12}$ rad/sec, which again compare well with our values (in 10^{12} Hz) of 1.3,2,2.2,3,3.1,3.4,3.8 and 4.2. The experimental sound speeds from $\Gamma - Z$ are also approximately equal to our calculated values, from comparison of the figures. All in all the good agreement suggests the accuracy and applicability of our lattice dynamics calculations on Bi_2Te_3.

For the lattice dynamics calculations LDA-optimized internal coordinates and lattice parameters (4.35 Åplanar, 29.82 Åc-axis) were used, while for the elastic constant calculations experimental lattice parameters of 4.386 Åplanar and 30.50 Åc-axis (but LDA-optimized internal coordinates) were employed. As is well known, van der Waals interactions can be important for layered materials such as Bi_2Te_3, and while these are not included in our functionals we do find good agreement with the experimental properties in the lattice dynamics calculations, as indicated. The elastic constant calculations (see Table 1) exhibit somewhat larger discrepancies with experiment (see Table 3), even with usage of the LDA, with (for example), the value of c_{12} calculated as 3.8 GPa, much smaller than the experimental value of 22.0 GPa. We ascribe this to the difficulty of incorporating all bonding effects in layered materials such as Bi_2Te_3 into the simple LDA. For these calculations we used between 182 and 770 k-points in the irreducible portion of the Brillouin zone (note that the elastically distorted Brillouin zone need not retain the hexagonal symmetry), employed spin-orbit coupling except for the optimizations, and LAPW sphere radii of 2.5 Bohr radii.

Since above we describe the effect of using the LDA for *structural* properties of layered semiconductors such as Bi_2Te_3, it is worthwhile to ask about the effect of using the LDA for *electronic* properties of Bi_2Te_3. Therefore in Figure 2 we present the calculated electronic structure of Bi_2Te_3 within both the GGA *and* LDA approximations (calculated using WIEN2K) where all other relevant quantities such as LAPW sphere radii (2.5 Bohr radii for all atoms), *k*-points (2000 in the full Brillouin zone), and lattice parameters (4.386 Åplanar and 30.50 Åc-axis) and atomic coordinates are assumed identical. We have used spin-orbit coupling for these calculations as this generally affects electronic structure much more substantially than structural properties.

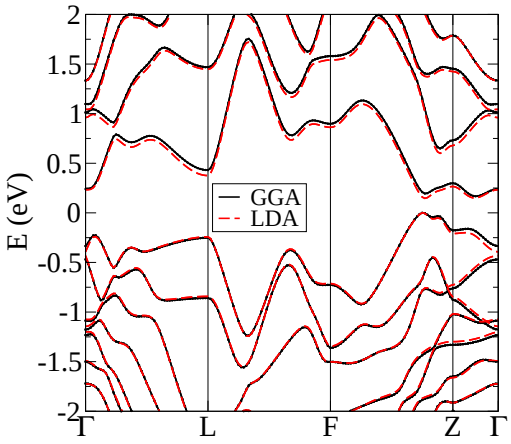

FIG. 2. The computed band structure of Bi_2Te_3 within the LDA and GGA approximations. Note the relatively small differences in the bandstructures.

As the plot indicates, there is only a very small difference between the two electronic structures, mainly concerning the exact value of the gap at the conduction band minimum.

III. SOUND SPEED ANISOTROPY AND NANOSTRUCTURING EFFECTIVENESS PARAMETERS

The discussion of the previous section makes plain the significant anisotropy in the phonon transport of Bi_2Te_3. Here we find a way to assess the quantitative impact of this anisotropy in reducing lattice thermal conductivity and make a comparison with another well-studied thermoelectric material, PbTe, as well as diamond and several other semiconductors

In this discussion we will implicitly assume that the grain boundary scattering is in the ballistic regime, which will obtain when the average phonon mean free path (that would occur in the absence of grain boundaries) becomes comparable to or larger than the grain size. More specifically, we will assume that at least a significant fraction of the distribution of these phonon mean free paths is larger than the nanograin size, so that there is significant ballistic scattering at the grain boundaries. In this limit the well-established acoustic mismatch theory[24–27] describing heat conduction at interfaces of crystalline solids can be applied, as is described below.

Our method is the following. From published calculated values of the elastic constants for Bi_2Te_3 one may generate the associated Christoffel[28] elastic tensor stiffnesses and solve the resulting secular equation for the three sound velocities (one longitudinal and two transverse) as a function of wave propagation direction. The relevant equations may be found in Ref 29, and are summarized in the Appendix. We have plotted up the sound speeds, as a function of propagation direction, in Figure 3. The sound speed plots differ significantly from a spherical shape, underscoring the anisotropy already apparent from the calculated phonon bandstructure.

We turn now to the impact of the anisotropic sound speeds on the lattice thermal conductivity. As is well known, the lattice thermal conductivity κ_l is given as

$$\kappa_l = \sum_{\mathbf{q},i} C_{\mathbf{q},i} v_{\mathbf{q},i} \ell_{\mathbf{q},i} \tag{2}$$

where $C_{\mathbf{q},i}$ is the specific heat attributable to a phononic mode with momentum $\mathbf{q}$ and polarization i, v the sound speed of that mode and ℓ the mean free path of that mode, and a sum over the modes of significant group velocity is taken. In general, the fraction R of elastic energy reflected at a grain boundary interface at normal incidence is given by the impedance mismatch

formula:

$$R = \left(\frac{(Z_1 - Z_2)}{(Z_1 + Z_2)} \right)^2 \tag{3}$$

Here Z_1 and Z_2 are the acoustic impedances of the two adjoining grains, given by $Z_i = \rho_i v_i$, where ρ is the density of a grain and v the sound speed (of a given polarization) within the grain. Since we expect ρ to be constant within a nanostructured sample, the energy fraction reflected depends on the sound speeds v_1 and v_2 in the two grains, *at the directions of incidence and transmission*, and in addition on the polarization of the incoming wave. Note also[30] that an incident wave of one polarization may induce scattered waves of other polarizations, complicating the issue further. Furthermore, in a nanostructured sample we do not expect oriented grains. Hence to work out the effective grain boundary scattering rate one must consider grain orientation as well as the intrinsic anisotropy of the sound speeds. This becomes a rather difficult, and even difficult to formulate, problem when one realizes that the grains are not likely to be exactly randomly oriented, and that the degree of randomness will likely depend on the exact synthesis and nanostructuring techniques applied, unknown in this work.

Given that one purpose of this paper is to propose computationally simple nanostructuring effectiveness parameters, we therefore make a simple ansatz based upon the (relatively) random nature of the problem at hand. Since the incident and transmitted velocities v_1 and v_2 are essentially uncorrelated, it is a fair approximation to replace v_2 in the above impedance mismatch expression by its average value (a similar assumption in a different context is made in many "mean-field" theories) and integrate over all angles of incidence. As with mean-field theories, the simpler expression is most quantitatively accurate when v_1 does not vary too much from its average. The gross features of anisotropy, however, should be reasonably well captured by this expression. The expression for R_{total} is a simple two-dimensional integral:

$$R_{total} = \frac{1}{4\pi} \int sin(\theta) d\theta d\phi \left(\frac{v(\theta,\phi) - v_{avg})}{(v(\theta,\phi) + v_{avg})} \right)^2 \tag{4}$$

where the above integral is computed for each of the two transverse modes and the longitudinal mode and then averaged over the modes. One could argue, based on phase space considerations, that the various terms should be weighted by the sound speeds, or sound speeds squared, or some other factor, of the various modes , but it is usually unclear in any given system what fraction of heat transport separately results from transverse and longitudinal modes[31], so we have retained the simplest possible expression.

The above expression yields a single number R_{total} which gives in essence the average impedance mismatch reflected energy *at normal incidence* for a single scattering event. It is typically fairly small - of the order of 0.01 or less even for highly anisotropic media, as depicted below. However, there is an important additional scattering effect created by the velocity anisotropy. As with propagation of electromagnetic waves, there is a form of Snell's law, $v_{incoming}/v_{transmitted} = \sin(\theta_{incoming})/\sin(\theta_{transmitted})$, relating incoming and outgoing propagation angles (relative to the normal) to the relative sound speeds, and a version of total internal reflection, in which for certain angles of incidence there is *no* energy transmission across the interface, applies. To put this quantitatively, for a 20 percent smaller sound speed (in a given direction) in the receiving material, angles of incidence greater than 53 degrees - *forty* percent of the possible angles of incidence - result in total internal reflection, even though the impedance mismatch reflection coefficient at normal incidence is only 0.012. This point is described well quantitatively in the reference of Little[9]. Since the *average* sound speeds in the two nanograins are of course equal, what one needs is a measure of the average deviation of the velocity from its average, which in essence is what the individual R_i measures (more precisely speaking $R_i \simeq \frac{(\Delta v_i)^2}{4v_{i,average}^2}$, where Δv is the standard deviation of v_i and $v_{average,i}$ the angular average sound velocity of a mode of polarization i.)

To give examples of velocity anisotropy and R_{total} we have computed and present in Figures 3, 4 and 5 the sound speed anisotropy for three well known semiconducting materials: Bi_2Te_3, diamond and PbTe respectively. Diamond is included to demonstrate a material with very low elastic anisotropy, while PbTe and $CoSb_3$ are well known thermoelectrics. We will see that as expected, Bi_2Te_3 shows significant potential for nanostructuring reductions of $\kappa_{lattice}$. As mentioned previously, despite its cubic structure, PbTe also shows large velocity anisotropy. As asserted previously, while its cubic nature ensures isotropic conductivity, there is no such requirement on the elastic properties. Its elastic anisotropy might therefore also be expected to allow good reductions of lattice thermal conductivity due to nanostructuring, but recent work[32] shows that for PbTe these nanostructures must be smaller than 10 nm to have a significant effect, as the phonon mean free path is already very short. Conversely, although diamond shows very low anisotropy, its phonon mean free path is so long (well over 100 nm) that small-grain nanostructuring would likely have a significant impact on its lattice thermal conductivity (noting nevertheless the impracticality of this material for thermoelectric applications). We have taken account of this additional effect by defining a "scattering potential coefficient" S_{total} as $R_{total}\kappa_{lattice,bulk}/\kappa_{min}$, where $\kappa_{lattice,bulk}$ is self explanatory (values for Bi_2Te_3 and PbTe taken from Ref. 21) and κ_{min} is the "minimum thermal conductivity"[33], which we simply take as 0.5 W/m-K for all materials studied.

In an attempt to quantify the anisotropy presented in Figs. 3-5, in Table 2 we present the average impedance mismatch scattering reflection coefficient R for each of the three materials, along with $CoSb_3$, GaAs and Si. As expected, diamond has by far the lowest impedance reflection coefficient, with an average R between one and two orders of magnitude less than PbTe

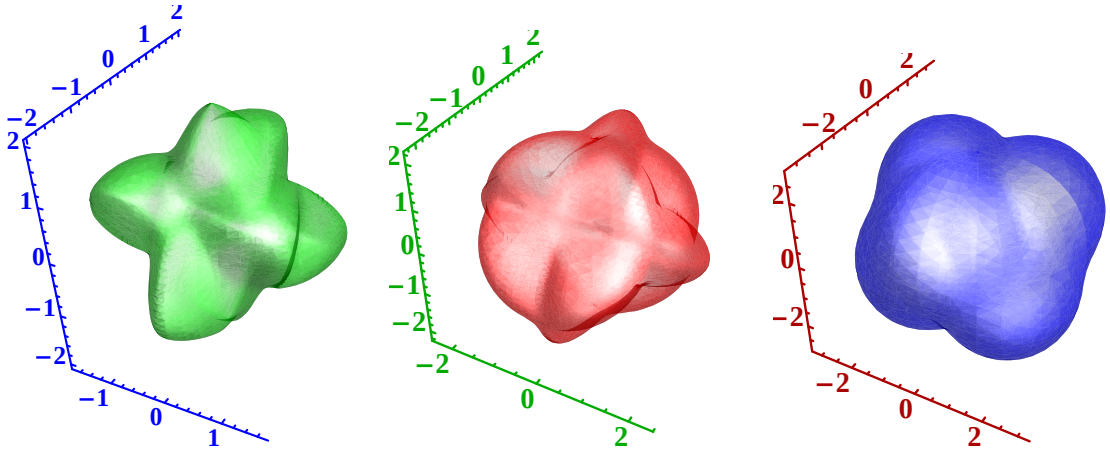

FIG. 3. The computed sound speed anisotropy of Bi_2Te_3. Distance from origin represents sound speed, in km/sec, for that direction of propagation. Transverse modes T1 and T2 left and center, respectively, longitudinal mode right. Elastic constants taken from Ref. 20.

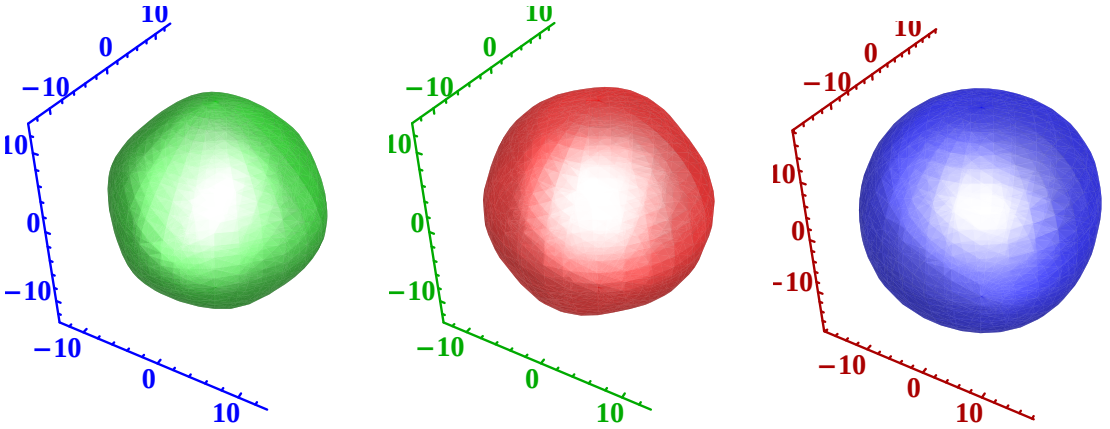

FIG. 4. The computed sound speed anisotropy of diamond. Elastic constants taken from Ref. 34. Transverse modes left and center, longitudinal mode right.

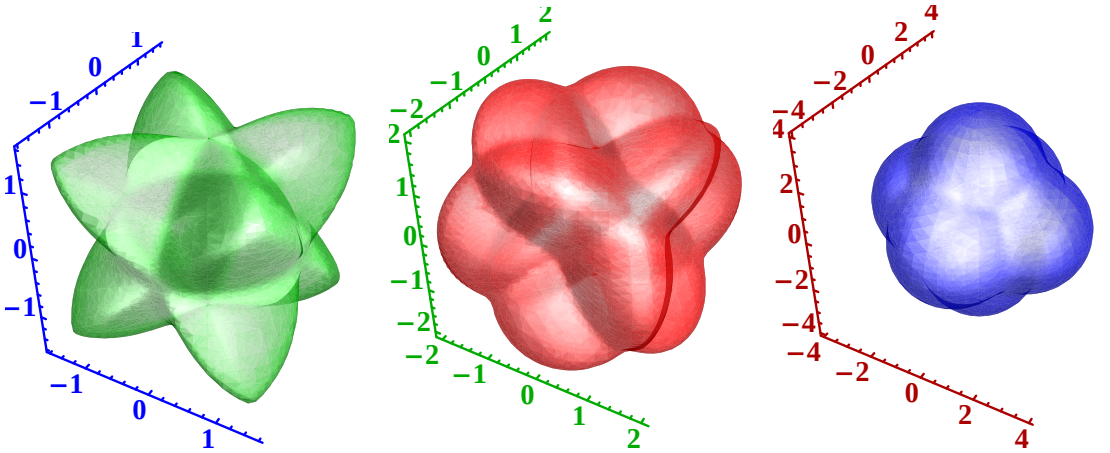

FIG. 5. The computed sound speed anisotropy of PbTe. Elastic constants taken from Ref. 35. Transverse modes left and center, longitudinal mode right.

and Bi_2Te_3. The large values for PbTe suggest that, as with Bi_2Te_3, nanostructuring may yet be effective in reducing $\kappa_{lattice}$, if sufficiently small nanograins can be formed. WIth regards to $CoSb_3$, note that while this material shows significant potential

TABLE II. Average impedance mismatch reflection coefficients (multiplied by 100), scattering potential coefficients, and experimental lattice thermal conductivity reductions, for several materials. L refers to the longitudinal mode and $T1$ and $T2$ to the transverse modes. The skutterudite values in parentheses indicate typical values for a high performance thermoelectric skutterudite.

Compound	R_L	R_{T1}	R_{T2}	R_{total}	$\kappa_{lattice,bulk}$ (W/m-K)	S_{total}	$\kappa_{lattice}$ reduction from nano/polycrystalline
Bi_2Te_3	0.153	0.429	0.437	0.340	1.7 (planar)	1.16	1.4[6]
PbTe	0.187	0.544	0.850	0.527	2.3	2.42	—
$CoSb_3$	0.0234	0.0623	0.133	0.0703	9 (3)	1.26 (0.42)	7[37]
diamond	0.00627	0.0151	0.00537	0.0089	2200	39.16	100[43]
GaAs	0.02621	0.04247	0.1436	0.0706	46[44]	6.51	38[45]
Si	0.01668	0.1436	0.04247	0.06766	156[46]	21.11	142[47]

TABLE III. Elastic constants (in GPA) used in the calculation of sound speed anisotropies. All compounds except for Bi_2Te_3, are cubic and hence have only three independent elastic constants.

Compound	c_{11}	c_{12}	c_{33}	c_{44}	c_{13}	c_{14}
Bi_2Te_3	74.4	22.0	51.6	31.4	29.2	15.4
PbTe	128.1	4.4	—	15.1	—	—
$CoSb_3$[36]	202.0	55.8	—	42.2	—	—
diamond	1076	125	—	576	—	—
GaAs[44]	118.4	53.7	—	59.1	—	—
Si[48]	166	64.0	—	79.6	—	—

for nanostructuring lattice thermal conductivity reduction (since S_{total} is substantial), this reduction would be proportionately smaller for a high performance skutterudite such as a triple-filled material, since the lattice term has already been reduced substantially by the 'rattling' effect. Hence high performance skutterudites would be expected to show smaller performance benefits from nanostructuring than PbTe and Bi_2Te_3. Conversely, as observed in Ref. 37, substantial $\kappa_{lattice}$ reductions - as much as 80 percent - occur in nanostructured $CoSb_3$ without added 'rattlers'. The very small values of R for diamond provide a natural explanation for why polycrystalline diamond is such a good heat conductor. We have not included the thermoelectric half-Heusler compounds due to a paucity of data and a great variability[38–42] in anisotropy in the few data that do exist. For Bi_2Te_3 the lattice thermal conductivity given is the planar value; the c-axis value is roughly half this.

IV. DISCUSSION AND PROPOSED EXPERIMENTAL TEST OF THEORY

The results of the previous section attempt to define a nanostructuring "figure-of-merit", the scattering potential coefficient S_{total} which we hypothesize will correlate with the ability of nanostructuring to reduce lattice thermal conductivity. In the last two columns of Table 3 we present the parameters S_{total} and the measured reduction in thermal conductivity, relative to single-crystal values, of nanostructuring or, in the absence of such data, of polycrystalline samples. There is an obvious correlation between the two parameters, but it is not clearly better[49] than a simple correlation between the measured thermal conductivity reduction and the single crystal thermal conductivity values; in particular, Bi_2Te_3 and $CoSb_3$, show very different $\kappa_{lattice}$ reductions despite nearly equal S_{total} values. The reason for this, we believe, is simply that the grain sizes in the nanostructured (or for that matter, polycrystalline) samples are not the same from one material to another, so that this is not an "apples-to-apples" comparison.

To make such a comparison, let us consider the thermal conductivity of a nanostructured sample with two sources of scattering: the phonon-phonon scattering commonly dominating $\kappa_{lattice}$ for temperatures above the Debye temperature, and grain boundary scattering from the nanograins. One may then write the total scattering rate, using Matthiesen's rule, as

$$\tau^{-1} = \alpha T + \beta v_s/d \tag{5}$$

Here α and β are material specific constants, d the mean grain size, and v_s a suitably averaged sound speed. β describes the efficacy of grain boundary scattering in a given material and α the effectiveness of phonon-phonon scattering. The sound speed appears in this expression because higher sound speeds imply shorter times to traverse a nano-grain and undergo a scattering event. Then one may write the thermal conductivity as

$$\kappa_{lattice} = \frac{C v_s^2}{\alpha(T + \frac{\beta v_s}{\alpha d})} \tag{6}$$

Here C is the specific heat, which we assume to be known. We may readily identify the quantity β/α with the scattering potential coefficient S_{total}, since in our theory β expresses the relative effect of impedance mismatch scattering, and α the effect of phonon-phonon scattering, which predominates $\kappa_{lattice}$ in bulk materials.

To test this assertion, what is needed are two or more sets of thermal conductivity measurements on materials with rather different S_{total} values, with each set comprising a series of tests of samples with nanograins of different sizes d. This would allow determination of the values of α/β for each of the two materials, which could then be compared with the calculated S_{total} values. One caveat is that the above expression for the scattering time fails as one approaches the minimum thermal conductivity, so that measurements at lower temperatures (say 300 K) would likely be more accurate since κ is larger at low temperature.

This represents an attempt to isolate the effects of velocity anisotropy scattering from the numerous other factors affecting phononic transport in a real nanostructured sample, including (for example) the means of sample preparation and other microstructural properties. In addition, other forms of scattering, such as by soft interstitial material between grains, could be a significant contributor to reducing thermal transport. We do think, however, that the impedance and velocity mismatch associated with grain boundary scattering in nanostructured samples, as depicted here, can be a significant contributor to the reduction of thermal conductivity by nanostructuring, and that the quantitative parameters presented may give an indication of the likely effectiveness of nanostructuring in reducing the lattice thermal conductivity of a given material.

V. SUMMARY AND CONCLUSIONS

We present calculated phonon dispersions for Bi_2Te_3 and discuss ceramic grain boundary scattering in terms of acoustic impedance mismatch. We find that as expected grain boundaries may lead to strong interface scattering in Bi_2Te_3 nanostructured material. Interestingly, this is also expected to be the case in materials such as PbTe, which although cubic does have substantial acoustic wave anisotropy. This is in contrast to the optical case, where a cubic material would have no such scattering. In any case, the implication of the present results is that dense sintered ceramics of anisotropic material such as Bi_2Te_3 or PbTe will have reduced thermal conductivity provided that the appropriate grain size is used; we develop a method for quantifying this velocity anisotropy. In the case of more isotropic materials other strategies for producing scattering at grain boundaries, such as the introduction of second phases (as studied in Refs. 50 and 51) may be needed.

Acknowledgments

This research was supported by the U.S. Department of Energy, EERE, Vehicle Technologies, Propulsion Materials Program (DP) and the Solid State Solar-Thermal Energy Conversion Center (S3 TEC), an Energy Frontier Research Center funded by the US Department of Energy, Office of Science, Office of Basic Energy Sciences under Award Number: DE-SC0001299/DE-FG02-09ER46577 (DJS).

VI. APPENDIX

In this section we describe in somewhat more detail the method for extracting sound speeds from the elastic constants. For the sake of brevity we will only demonstrate the most complex case depicted in the manuscript, that of rhombohedral Bi_2Te_3. In general, solving the Christoffel equations requires the solution of a 3x3 determinant equation, $\det[\Gamma - \lambda \mathbf{1}] = 0$. Here the eigenvalues λ are equal to $\rho v^2_{i,\theta,\phi}$, where ρ is the material density and $v_{i,\theta,\phi}$ the sound speed of given polarization and propagation. The matrix Γ is the elastic stiffness matrix. For Bi_2Te_3 there are six nonzero elastic constants: $c_{11}, c_{12}, c_{13}, c_{14}, c_{33}$ and c_{44}. Then the components of the symmetric Γ matrix are given as follows[28] (here n_1, n_2 and n_3 are the direction cosines along the x, y and z axes which we take in spherical coordinates):

$$\Gamma_{11} = n_1^2 c_{11} + \frac{n_2^2}{2}(c_{11} - c_{12}) + n_3^2 c_{44} + 2n_2 n_3 c_{14} \tag{7}$$

$$\Gamma_{22} = n_2^2 c_{22} + \frac{n_1^2}{2}(c_{11} - c_{12}) + n_3^2 c_{44} - 2n_2 n_3 c_{14} \tag{8}$$

$$\Gamma_{33} = n_2^2 c_{44} + n_2^2 c_{44} + n_3^2 c_{33} \tag{9}$$

$$\Gamma_{23} = \Gamma_{32} = (n_1^2 - n_2^2) c_{14} + n_2 n_3 (c_{13} + c_{44}) \tag{10}$$

$$\Gamma_{13} = \Gamma_{31} = n_1 n_3 (c_{13} + c_{44}) + 2n_1 n_2 c_{14} \tag{11}$$

$$\Gamma_{23} = \Gamma_{32} = n_1 n_3 c_{14} + n_1 n_2 (c_{11} + c_{12})/2 \tag{12}$$

Diagonalization of Γ then directly yields the eigenvalues λ and associated sound speeds $v_{i,\theta,\phi}$.

[1] G.A. Slack, *CRC Handbook of Thermoelectrics*, ed. D.M. Rowe, pp. 407 40. Boca Raton, FL: CRC Press, 1995.
[2] B.C. Sales, D. Mandrus and R.K. Williams, Science **272**, 1325 (1996).
[3] T. He, J. Chen, H.D. Rosenfeld and M.A. Subramanian, Chem. of Mat. **18**, 759 (2006).
[4] X. Shi, S. Bai, L. Xi, J. Yang, W. Zhang, L. Chen and J. Yang, J. Mat. Res. **26**, 1745 (2011).
[5] B. Poudel, Q. Hao, Y. Ma, Y. Lan, A. Minnich, B. Yu, X. Yan, D. Wang, A. Muto, D. Vashaee, X. Chen, J. Liu, M. S. Dresselhaus, G. Chen, and Z. Ren, Science **320**, 634 (2008).
[6] W. Xie, X. Tang, Y. Yan, Q. Zhang and T.M. Tritt, Appl. Phys. Lett. **94**, 102111 (2009).
[7] D. Parker and D.J. Singh, Phys. Rev. X **1**, 021005 (2011).
[8] H. Jiang, Y.K. Zou, Q. Chen, K.K. Li, R. Zhang, Y. Wang, H. Ming and Z. Zheng, Proc. SPIE **5644**, 380 (2005).
[9] W. A Little, Can. J. Phys. **37**, 334 (1959).
[10] E.T. Swartz and R.O. Pohl, Rev. Mod. Phys. **61**, 605 (1989).
[11] G. Kresse and D. Joubert, Phys. Rev. B **59**, 1758 (1999).
[12] Vienna Ab-initio Simulation Package, available from www.vasp.at.
[13] B. Qiu and X. Ruan, Phys. Rev. B **80**, 165203 (2009).
[14] B.-L. Huang and M. Kaviany, Phys. Rev. B **77**, 125209 (2008).
[15] B.-T. Wang and P. Zhang, Appl. Phys. Lett. **100**, 082109 (2012).
[16] W. Kullmann, G. Eichhorn, H. Rauh, R. Geick, G. Eckold and U. Steigenburger, Phys. Stat. Sol. **162**, 125 (1990)
[17] J.P. Perdew, J.A. Chevary, S.H. Vosko, K.A. Jackson, M.R. Pederson, D.J. Singh and C. Fiolhais, Phys. Rev. B **46**, 6671 (1992).
[18] J.P Perdew and Y. Wang, Phys. Rev. B **45**, 13244 (1992).
[19] P. Blaha, K. Schwarz, G. K. H. Madsen, D. Kvasnicka and J. Luitz, WIEN2k, An Augmented Plane Wave + Local Orbitals Program for Calculating Crystal Properties
[20] J.O. Jenkins, J.A. Rayne and R.W. Ure, Jr., Phys. Rev. B **5**, 3171 (1972).
[21] D.P. Spitzer, J. Phys. Chem. Sol. **31**, 19 (1970).
[22] L. Fast, R. Ahuja, L. Nordström, J.M. Wills, B. Johannson and O. Eriksson, Phys. Rev. Lett. **79**, 2301 (1997).
[23] M.J. Mehl, Phys. Rev. B **47**, 2493 (1993).
[24] F. Nitsche and B. Schumann, J. Low Temp. Phys. **39**, 119 (1980).
[25] R.E. Peterson and A.C. Anderson, J. Low Temp. Phys. **11**, 639 (1973).
[26] W. Kappus and O. Weis, J. Appl. Phys. **44**, 1947 (1973).
[27] P. Herth and O. Weis, Z. Angew. Phys. **29**, 101 (1970).
[28] M.J.P. Musgrave, *Crystal Acoustics*, Acoustic Soc. of America, 2003.
[29] W.G. Meyer and P.M. Parker, Acta Cryst. **14**, 725 (1961).
[30] W. M. Ewing, *Elastic Waves in Layered Media*, (McGraw-Hill: New York), 1957.
[31] A Callaway-type expression $\kappa_{lattice} = Cv\ell$ would suggest that the higher velocity longitudinal mode would be the largest contributor to thermal transport, but this is offset by the smaller region of phase space in which this sound velocity applies due to the intersection with optical branches (see Fig. 1) so that the ultimate apportionment of heat transfer amongst the various modes is not a trivial matter.
[32] T. Shiga, J. Shiomi, J. Ma, O. Delaire, T. Radzynski, A. Lusakowski, K. Esfarjani and G. Chen, Phys. Rev. B **85**, 155203 (2012).
[33] G.A. Slack, Solid State Physics **34**, 1 (1979).
[34] M.H. Grimsditch and A.K. Ramdas, Phys. Rev. B **11**, 3139 (1975).
[35] B. Houston, R.E. Strakna and H.S. Belson, J. Appl. Phys .**39**, 3913 (1968).
[36] J.L. Feldman and D.J. Singh, Phys. Rev. B **53**, 6273 (1996).
[37] J.L. Mi, T.J. Zhu, X.B. Zhao and J. Ma, J. Appl. Phys. **101**, 054314 (2007)
[38] M. Hichour, D. Rached, R. Khenata, M. Rabah, M. Merabet, A.H. Reshak. S.B. Omran and R. Ahmed, J. Phys. Chem. Sol. **73**, 975 (2012).
[39] A. Hamidani, B. Bennecer and B. Boutarfa, Mat. Chem. and Phys. **114**, 732 (2009).
[40] B. Kong, X.-R. Chen, J.-X. Yu and C.-L. Cai, J. All. Comp. **509**, 2611 (2011).
[41] Y. Kawaharada, K. Kurosaki, H. Muta, M. Uno and S. Yamanaka, J. All. Comp. **381**, 9 (2004).
[42] L. Manosa, A. Gonzalez-Comas, E. Obrado, A. Planes, V.A. Chernenko, V.V. Kokorin and E. Cesari, Phys. Rev. B **55**, 11068 (1997).
[43] J.E. Graebner, S. Jin, G.W. Kammlott, J.A. Herb and C.F. Gardinier, Appl. Phys. Lett. **60**, 1576 (1992).
[44] R.I. Cottam and G.A. Saunders, J. Phys. C: Sol. State Phys. **6**, 2105 (1973).
[45] S.P.R. Clark, P. Ahirwar, F.T. Jaeckel, C.P. Hains, A.R. Albrecht, T.J. Rotter, L.R. Dawson, G. Balakrishnan, P.E. Hopkins, L.M. Phinney, J. Hader and J.V. Moloney, J. Vac. Sci. Tech. B **29**, 03C130 (2011).
[46] C.J. Glassbrenner and G.A. Slack, Phys. Rev. **134**, A1058 (1964).
[47] S. Uma, A.D. McConnell, M. Asheghi, K. Kurabayashi and K.E. Goodson, Int. J. Thermophys. **22**, 605 (2001).
[48] H.J. McSkimmin and P. Andreatch, J. Appl. Phys. **35**, 2161 (1964).
[49] Note that the work of Ref. 43 in fact depicts a lattice thermal conductivity which varies significantly with grain size. For ease of comparison we have chosen the value from the largest grain size.
[50] J. Androulakis, C.-H. Lin, H.-J. Kong, C. Uher .C.-I. Wu, T. Hogan, B.A. Cook, T. Caillat, K. Paraskevopoulos and M.G. Kanatzidis, J. Am. Chem. Soc. **129**, 9780 (2007).
[51] K. Biswas, J. He, G. Wang, S.-H. Lo, C. Uher, V.P. Dravid and M.G. Kanatzidis, Ener. and Env. Sci. **4**, 4675 (2011).